Available online at www.sciencedirect.com
SCIENCE DIRECT
Polymer 47 (2006) 2423–2433
polymer
www.elsevier.com/locate/polymer

Solid state structure and oxygen transport properties of copolyesters based on smectic poly(hexamethylene 4,4′-bibenzoate)

Y.S. Hu [1], A. Hiltner *, E. Baer

Department of Macromolecular Science and Engineering, Center for Applied Polymer Research, Case Western Reserve University, Cleveland, OH 44106-7202, USA

Received 3 December 2005; received in revised form 26 January 2006; accepted 27 January 2006
Available online 28 February 2006

Abstract

This study examined the solid state structure and oxygen barrier properties of copolyesters based on smectic poly(hexamethylene 4,4′-bibenzoate) (PHBB) and non-liquid crystalline poly(hexamethylene isophthalate) (PHI). The isophthalate content was varied from 10 to 75 mol%. Differential scanning calorimetry (DSC), wide angle X-ray diffraction (WAXD), dynamic mechanical thermal analysis (DMTA), and atomic force microscopy (AFM) were employed to characterize the polymers. The strong ordering tendency of 4,4′-bibenzoate was demonstrated by the persistence of ordered PHBB structures in copolymers with large amounts of the kinked isophthalate comonomer. Copolymers with up to 50 mol% isophthalate gave evidence of liquid crystalline (LC) character in the precursor melt. Copolymers with up to 75 mol% isophthalate crystallized in the PHBB α-crystal form with only small perturbations of the unit cell. The copolymers provided insight into the low gas permeability of LC polymers. Changes in both solubility and diffusivity contributed to the lower oxygen permeability of the smectic glass compared to the amorphous glass. Smaller free volume hole size of the smectic glass gave rise to lower oxygen solubility and contributed to lower diffusivity. The extended chain conformation in the smectic glass, which reduced the fraction of glycol units in gauche conformations, was a second factor that contributed to lower diffusivity.

Keywords: Liquid crystal polymer; Polyesters; Oxygen transport

1. Introduction

Thermotropic liquid crystalline polymers (LCPs) have been of interest as engineering plastics because of their low viscosity and ease of orientation, their high-strength, and their high barrier performance. The low gas permeability of LCPs stems mainly from low solubility rather than from low diffusivity [1–4]. Other studies reveal the LC glass to have smaller free volume hole size than the amorphous glass [5,6]. If gas solubility is viewed as the process of filling holes of excess free volume, it follows that LC order leads to inherently low gas solubility.

Copolymerization is widely used to extend the structure–property spectrum of polymers in general. Copolymers in which the amount of LC character can be systematically changed are attractive for examining the role of LC character in achieving low gas permeability. This can be readily achieved by copolymerization with a non-mesogenic unit. Of the many possibilities, copolyesters based on 4,4′-bibenzoate offer several advantages. Bibenzoate readily undergoes polycondensation with a variety of diol spacers to form polyesters with smectic order [7]. Moreover, a surprisingly large fraction of a non-LC comonomer can be incorporated before LC behavior is completely lost. For example, poly(ethylene terephthalate-*co*-4,4′-bibenzoate) with up to 65 mol% terephthalate retains some LC-like behavior [8]. Finally, the polymers are tractable and can be fabricated from the melt into films and fibers.

The bibenzoate polyesters often crystallize from the smectic state. Recent studies of polyesters with 5-atom spacers, specifically poly(pentamethylene 4,4′-bibenzoate) (PP5BB) and poly(diethylene glycol 4,4′-bibenzoate) (PDEGBB) found that oxygen transport properties supported a simple two-phase model of impermeable crystallites dispersed in a permeable smectic glass [9,10]. Due to the low crystallite aspect ratio, crystallization only slightly increased the tortuosity of the diffusion pathway. Bibenzoate polyesters with even-numbered spacers crystallize more readily [11]. Poly(hexamethylene 4,4′-bibenzoate) (PHBB) has been well

* Corresponding author.
E-mail address: pah6@case.edu (A. Hiltner).
[1] Present address: The Dow Chemical Company, Freeport, TX 77541, USA.

0032-3861/$ - see front matter © 2006 Elsevier Ltd. All rights reserved.
doi:10.1016/j.polymer.2006.01.089

characterized [12,13]. Depending on the thermal history, three crystal forms have been described for PHBB, α, β and γ [14,15]. The present study examines the solid state structure and oxygen transport properties of copolyesters of 4,4′-bibenzoate and isophthalate with the hexamethylene spacer. A structural model is extracted from the combined results of thermal behavior, WAXD, dynamic mechanical response, and morphology by AFM. The structural model is the basis for understanding the oxygen transport properties of this family of polyesters.

2. Materials and methods

Poly(hexamethylene 4,4′-bibenzoate) (PHBB), poly(hexamethylene isophthalate) (PHI) and their copolymers with 10, 30, 50 and 75 mol% isophthalate were provided by KoSa (Spartanburg, SC) in the form of extruded pellets. The chemical structure of the copolymers is

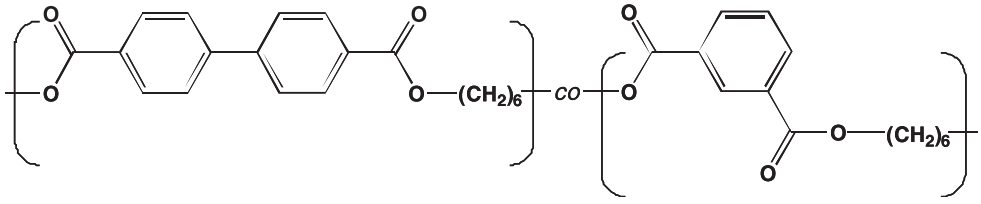

The copolymers are identified as PHBB-*x*I where *x* is the mole percent isophthalate. Randomization of copolymers was virtually ensured under the melt-polymerization conditions that were utilized [5]. The comonomer content is given as the reaction feed.

After the pellets were dried in vacuo for 24 h at a temperature in between ambient and 80 °C depending on the comonomer content, they were compression molded between Teflon-coated aluminum sheets in a press at 150–280 °C to obtain films 180–200 μm thick. Quenched films were taken rapidly from the isotropic melt into ice water. It was not possible to quench PHBB, PHBB-10I, PHBB-30I and PHBB-50I to the amorphous state due to the extremely rapid liquid crystalline and crystalline transitions. It was possible to quench PHBB-75I and PHI to the amorphous state; however, they underwent cold crystallization when stored at ambient temperature due to their low glass transition temperature (T_g), as evidenced by the clear films turning opaque with time. The crystallization was complete in about 3 weeks. Quenched films of copolymers with up to 50% isophthalate were used for characterization unless otherwise indicated. Films used to characterize PHBB-75I and PHI were quenched and aged at ambient conditions for 3 weeks unless otherwise indicated.

Thermal analysis was conducted with a Perkin–Elmer DSC-7 (Boston, MA) calibrated with indium and tin. Dynamic mechanical measurements were carried out in a dynamic mechanical thermal analyzer (DMTA) Mk II unit from Polymer Laboratories (Amherst, MA) operating in the tensile mode, using a frequency of 1 Hz and heating rate of 3 °C min^{-1}.

Wide-angle X-ray diffraction (WAXD) patterns were obtained at ambient temperature with a Philips diffractometer (Natick, MA) in the transmission mode using a slit angle of 1/12 °.

A film specimen for atomic force microscopy (AFM) was vacuum-dried, re-melted under nitrogen, and quenched in air. The surface was etched with 40 wt% aqueous methylamine solution at 23 °C. The optimum etching time was 12 h for PHBB, 1.5 h for PHBB-10I, 35 min for PHBB-30I and PHBB-50I, and 10 min for PHBB-75I and PHI. The etched specimens were washed with de-ionized water and methanol. Initially the specimens were about 35–50 μm in thickness. Etching removed material from the surface to a depth of about 150–400 nm. Images of the etched surfaces were obtained in air at ambient conditions using the Nanoscope IIIa MultiMode head from Digital Instruments (Santa Barbara, CA) in the tapping mode. The procedure was described previously [5,9].

Density was measured at 23 °C with a density gradient column constructed from an aqueous solution of calcium nitrate in accordance with ASTM-D 1505 Method B. Small pieces of film (~25 mm^2) were placed in the column and allowed to equilibrate for 30 min before measurements were taken.

Positron annihilation lifetime spectroscopy (PALS) was performed using a conventional fast–fast coincidence system. The instrumentation and procedures for data analysis were described previously [16].

Oxygen flux $J(t)$ at 23 °C, 0% relative humidity and 1 atm pressure was measured with a MOCON OX-TRAN 2/20 (Minneapolis, MN). The instrument was calibrated with NIST-certified Mylar® film of known oxygen transport characteristics. Specimens were carefully conditioned as described previously in order to obtain the non-steady state oxygen flux from which the diffusivity D was determined [17]. To obtain the diffusivity D and to accurately determine the permeability P, the data were fit to the solution of Fick's second law with appropriate boundary conditions

$$J(t) = \frac{Pp}{l}\left[1 + 2\sum_{n=1}^{\infty}(-1)^n \exp\left(-\frac{D\pi^2 n^2 t}{l^2}\right)\right] \quad (1)$$

The average thickness l of each specimen was determined as $l = W(A\rho)^{-1}$, where W is the specimen weight, A is the specimen area and ρ is the density. Solubility S was calculated from the relationship $S = PD^{-1}$.

3. Results and discussion

3.1. Slow cooling

The thermograms in Fig. 1 were obtained by cooling from 285 to 0 °C at a rate of 2 °C min^{-1}, followed by heating at a

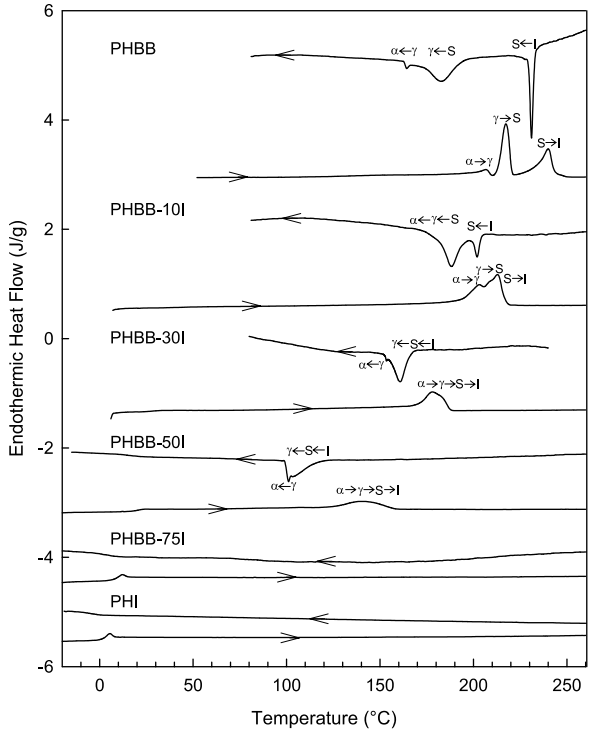

Fig. 1. Thermograms of PHBB, PHBB-I copolymers and PHI cooled from the isotropic melt to the glassy state at 2 °C min^{-1} and reheated at 10 °C min^{-1}. The cooling thermograms were normalized to 10 °C min^{-1} to facilitate comparison.

rate of 10 °C min^{-1}. Interpretation of the thermograms of the homopolymer PHBB readily followed from previous reports [7,11,12]. A sharp peak in the cooling curve at 231 °C with an exothermic heat of 29 J g^{-1} corresponded to the isotropic to smectic transition (I→S). It was followed by the smectic to γ-crystal transition (S→γ) at 183 °C with an exothermic heat of 36 J g^{-1}. The γ-crystal subsequently reorganized into the α-crystal (γ→α) as indicated by a small exotherm at 164 °C. The α-crystal form of PHBB after slow cooling was confirmed with WAXD, Fig. 2. Sharp crystalline reflections at 2θ values of 12.1, 15.5, 18.1, 19.7, 23.0, 24.3, 25.7 and 29.0° were

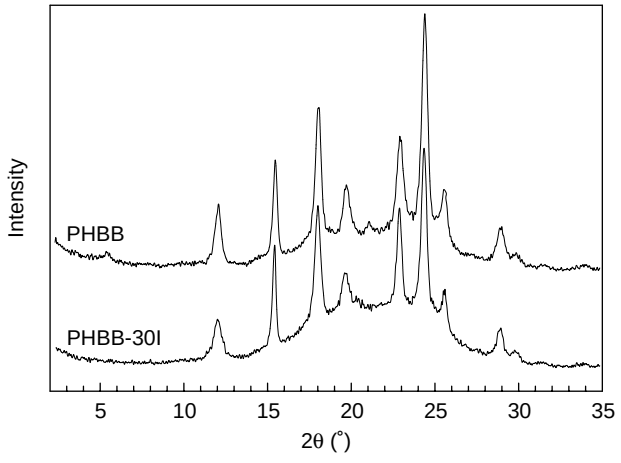

Fig. 2. WAXD scans of PHBB and PHBB-30I films slowly cooled through isotropic-to-smectic and smectic-to-crystalline transitions.

characteristic of the α-crystal form [14,15]. The weak peak at 5.55° (15.9 Å) corresponded to the distorted smectic layer spacing. The subsequent heating curve of PHBB showed the α→γ transition as a shoulder at 210 °C on the sharp γ→S endothermic peak at 218 °C. The endothermic S→I transition followed at 240 °C.

The cooling thermogram of PHBB-10I showed the I→S transition at 202 °C with exothermic heat of 24 J g^{-1}. Not surprisingly, the transition temperature and the exothermic heat were lower than for the homopolymer PHBB. The I→S transition was followed by a larger exotherm at 188 °C with an exothermic heat of 30 J g^{-1}. This was interpreted as the S→α transition with the α→γ transition appearing as a small shoulder on the low temperature side of the peak. The subsequent heating curve revealed three overlapping peaks centered at 203, 208 and 212 °C, corresponding to α→γ, γ→S and S→I transitions, respectively.

The cooling thermogram of PHBB-30I exhibited a large peak at 161 °C with a small shoulder at 153 °C. The enthalpy of 35 J g^{-1} was too large for this to be the I→S transition. Either PHBB-30I did not form a smectic phase and this peak was the I→γ transition, or, if PHBB-30I did form a smectic phase, this peak combined the I→S and S→γ transitions. The small shoulder was identified as the γ→α transition. The α-crystal form of PHBB-30I after slow cooling was confirmed with WAXD, Fig. 2. The heating curve of PHBB-30I revealed a complex enothermic peak at about 180 °C that could have encompassed the α→γ, γ→S and S→I transitions. The thermograms of PHBB-50I resembled those of PHBB-30I with lower transition temperatures and lower enthalpies. The suggested transition assignments were the same as for PHBB-30I. Cooling and heating thermograms of PHBB-75I and PHI showed only the glass transition at 8 and 1 °C, respectively.

In general, increasing isophthalate content caused the transition peaks to broaden, to shift to lower temperature and to decrease in enthalpy. In addition, increasing isophthalate caused the temperature interval between the I→S and S→γ transitions to become smaller until, for PHBB-30I and PHBB-50I, they merged into a single peak. As a consequence, it was not possible to determine from the thermograms whether these copolymers crystallized from the smectic form or from the isotropic melt. These trends reflected the progressive decrease in length and concentration of hexamethylene 4,4′-bibenzoate sequences. It should also be noted that copolymers with up to 50% isophthalate readily crystallized with the PHBB crystal forms including the distinct γ→α crystal transition.

3.2. Quenching

Quenching a PHBB film from the isotropic melt resulted in the γ-crystal form, Fig. 3, as indicated by broad reflections at 2θ of 13.7, 19.7 and 21.2° in the WAXD pattern [14,15]. A sharp peak at 2θ = 4.70° (18.8 Å) corresponded to the spacing of the smectic layers [18]. The spacing was less than the calculated length of the fully extended repeat unit of 19.62 Å [15]. The difference was attributed to the presence of some

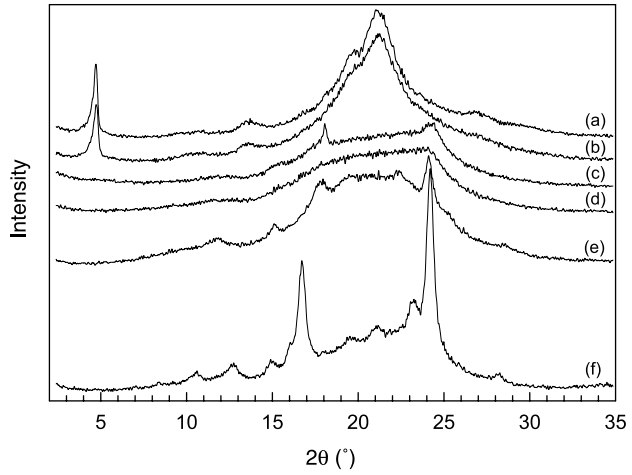

Fig. 3. WAXD scans of films quenched from the isotropic melt: (a) PHBB; (b) PHBB-10I; (c) PHBB-30I; (d) PHBB-50I; (e) PHBB-75I and (f) PHI. PHBB-75I and PHI were aged at ambient temperature for 3 weeks after quenching.

gauche or eclipsed conformations of the spacer [19,20]. The γ-crystal form and the smectic layer spacing were the same for PHBB-10I, although the γ-crystal reflections were broader than in PHBB and the layer reflection at 4.70° was slightly less intense.

In contrast, the WAXD patterns of quenched PHBB-30I and PHBB-50I showed poorly defined α-form reflections at 18.1 and 24.3° superimposed on a broad amorphous peak, Fig. 3. A reflection corresponding to the smectic layer spacing was missing. The loss of the smectic layer spacing from the α-crystal form appeared to be a general phenomenon (Fig. 2). This may be because the α-crystal has the fully extended chain conformation with a fiber repeat of 19.62 Å and unit cell density of 1.307 g cm^{-3}, whereas the γ-crystal has a less extended chain with a shorter fiber repeat of 19.39 Å and lower unit cell density of 1.254 g cm^{-3} [15]. Thus the chain configuration in the γ-form is closer to the configuration in the smectic phase with layer spacing of 18.8 Å. It may be possible for γ-crystals to coexist with the smectic phase, whereas transformation to α-crystals requires larger axial shifts that disrupt the smectic order.

Quenched PHBB-75I and PHI were amorphous and rubbery. They slowly underwent conventional cold-crystallization at ambient temperature. Surprisingly, the crystalline reflections of PHBB-75I resembled those of the PHBB α-crystal with a shift to lower angles of about 0.2°, which possibly accommodated insertion of comonomer units. A new crystal form was obtained for PHI with strong peaks at 16.7 and 24.2°. The estimated weight fraction crystallinity (ϕ_w) based on the WAXD pattern is listed in Table 1. The value of ϕ_w decreased with comonomer content from 0.29 for quenched PHBB to 0.13 for quenched PHBB-50I. Slow crystallization of PHBB-75I and PHI at ambient temperature resulted in crystallinities of 0.21 and 0.45, respectively. The glass transition temperature (T_g) and total enthalpy (ΔH_{total}) of the combined crystal and smectic transitions are also compiled in Table 1.

The density is included in Table 1. Usually, a density decrease accompanies the loss in LC character [6]. The surprisingly high density of PHBB-30I and PHBB-50I was attributed to the higher unit cell density of the α-crystal form in PHBB-30I and PHBB-50I compared to the γ-crystal form in quenched PHBB and PHBB-10I.

The DMTA curves of quenched films in Fig. 4 show the β-relaxation region as storage modulus (E'), loss modulus (E'') and loss tangent (tan δ). The glass transition, taken as the tan δ peak temperature [21,22], was about 10 °C higher than the glass transition temperature in DSC scans, Table 1. The peak temperature of 59 °C for PHBB was in good agreement with the literature report [7].

The low relaxation strength of the PHBB and PHBB-10I tan δ peaks was typical of crystalline LCPs [10]. The more intense tan δ response of PHBB-30I consisted of a lower temperature peak at about 33 °C with a shoulder at about 50 °C. The complex tan δ peak suggested that the non-crystalline regions of PHBB-30I possessed both amorphous and LC characteristics. Possibly the lower temperature peak arose from disordered amorphous chains and the higher temperature shoulder revealed some persisting LC character in the non-crystalline phase. The tan δ response of PHBB-50I showed a strong peak at 31 °C. The intensity of 1.2 was comparable to that of a typical amorphous polymer, which suggested that any LC character of PHBB-50I in the melt was lost when the polymer crystallized. The lower tan δ peak intensities of PHBB-75I and PHI were consistent with the relatively high levels of crystallinity attained during aging at ambient temperature.

It is characteristic of the non-crystalline LC phase that the free volume holes are smaller than in a conventional amorphous phase. This trend was seen for the quenched PHBB-I copolymers in Fig. 5. The smallest hole sizes were measured for PHBB and PHBB-10I, which was consistent with the LC nature of the non-crystalline phase. The hole size of PHBB-30I was intermediate between amorphous and LC, which was consistent with the partial LC nature of the non-crystalline regions inferred from the shape and intensity of the β-relaxation. The hole size of PHBB-50I was almost as large as that of PHBB-75I and PHI, which indicated that the non-crystalline regions were amorphous in agreement with the intense DMTA β-relaxation.

3.3. Morphology

The morphology of the PHBB-I copolymers was probed with specimens that were quenched from the isotropic melt to ambient temperature. A 2 μm AFM phase image of the etched PHBB surface revealed domains on the 0.5 μm size scale, Fig. 6(a). The supermolecular texture within the domains consisted of arrays of lamellae. Such lamellar structures are typical of smectic and nematic LCPs [5,9,23–26]. The lamellar thickness of 20 nm was consistent with the lamellar dimension reported previously for PHBB [27–29]. Domains of PHBB-10I were smaller, about 0.1–0.5 μm in size, Fig. 6(b). Arrays of very fine lamellae with thickness of 12 nm made up the

Table 1
Physical properties of quenched PHBB-I copolymers

Polymer	Density (g cm^{-3})	T_g (°C)			ϕ_w (WAXD)	P (cm^3(STP) cm m^{-2} atm^{-1} day^{-1})	D_2 (10^{-13} m^2 s^{-1})	S (cm^3(STP) cm^{-3} atm^{-1})	S_m (cm^3(STP) cm^{-3} atm^{-1})	ΔH_{total} (J g^{-1})	Free volume hole radius (Å)
		DSC	DMTA tan δ	DMTA E''							
PHBB	1.2469±0.0008	48	59	50	0.29	0.0906±0.0008	7.3±0.1	0.0141±0.0001	0.020	57	2.48
PHBB-10I	1.2444±0.0014	43	54	46	0.24	0.116±0.004	8.0±0.1	0.0168±0.0006	0.022	45	2.48
PHBB-30I	1.2436±0.0006	32	33, 50	32	0.18	0.169±0.009	8.4±0.3	0.0232±0.0021	0.028	33	2.54
PHBB-50I	1.2298±0.0008	22	31	27	0.13	0.351±0.011	12.2±0.7	0.0332±0.0014	0.038	24	2.63
PHBB-75I[a]	1.2093±0.0004	7	18	10	0.21	1.12±0.01	33.1±0.6	0.0393±0.0017	0.050	16	2.66
PHI[a]	1.2396±0.0009	4	12	7	0.45	0.615±0.007	30.5±0.5	0.0233±0.0010	0.042	41	2.68

[a] Quenched and aged for 3 weeks.

domains. Although PHBB and PHBB-10I crystallized during quenching, it appeared that crystallization occurred by transformation within the LC lamellae, leaving the domain structure largely undisturbed.

The AFM image of PHBB-30I exhibited densely packed, short curving lamellae about 11–12 nm thick, Fig. 6(c). Such densely packed lamellar textures were often seen in smectic 4,4′-bibenzoate polyesters when rapid cooling from the melt or the presence of a non-LC comonomer prevented formation of well-defined domains [5,9,10]. In this case, the non-crystalline regions retained some smectic character as inferred from the DMTA and PALS results. Surprisingly, a similar lamellar texture was observed in PHBB-50I, Fig. 6(d). Considering the small amount of crystallinity in quenched PHBB-50I,

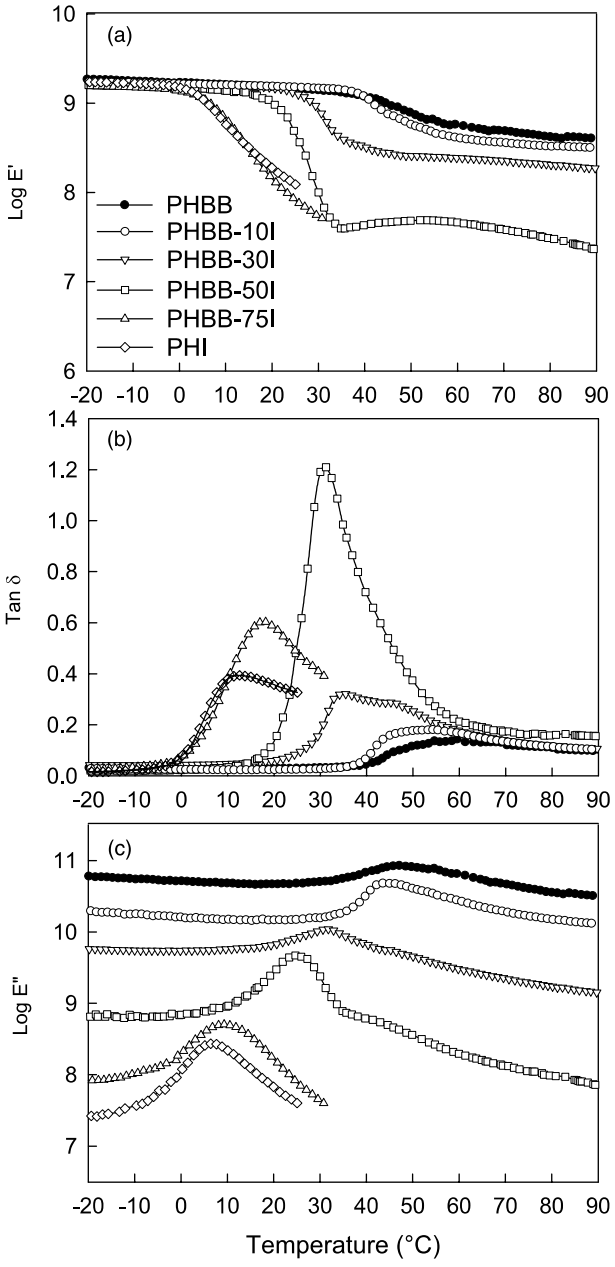

Fig. 4. DMTA curves showing the β-relaxation region: (a) log E'; (b) tan δ; (c) log E''. The E'' curves are shifted vertically.

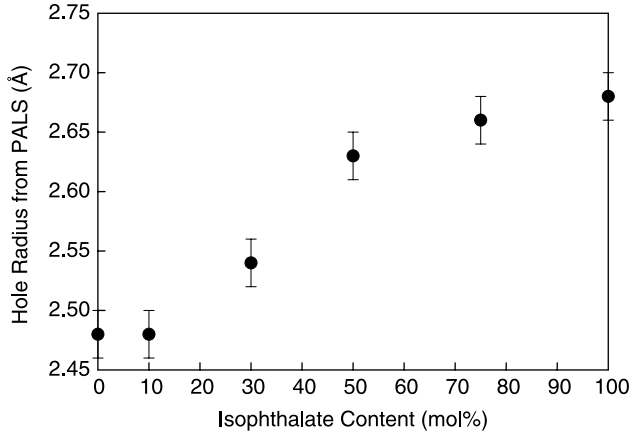

Fig. 5. Effect of isophthalate content on the free volume hole size from PALS.

crystallization from the isotropic melt would not produce this level of lamellar organization. Rather, it suggested that PHBB-50I crystallized from a melt with some smectic order. However, in this case, the non-crystalline regions of the quenched film were amorphous with no discernable smectic character.

The AFM images of rubbery PHBB-75I and PHI obtained immediately after quenching from the melt were virtually featureless. After slowly crystallizing at ambient temperature, PHBB-75I showed crystalline lamellae organized into spherulite-like structures, Fig. 6(e). The lamellar thickness was 13–15 nm. Well-formed and impinging spherulites on the size scale of 20 μm dominated the morphology of crystallized PHI, Fig. 6(f).

3.4. Structure model

The structural model for quenched PHBB is typical for a smectic polyester of bibenzoic acid [5,9]. More or less extended chains assemble with the mesogenic bibenzoate groups organized into smectic layers. The spacing of the smectic layers in this case is 18.8 Å from WAXD, which is less than the extended chain dimension, estimated at 19.62 Å. Stacks of smectic layers form the lamellae seen in the AFM images. The lamellar thickness of 20 nm corresponds to a stack with 11 smectic layers. Assemblies of lamellae constitute domains on the micron size scale.

Combined results from DSC, WAXD, DMTA and AFM indicate the 10 mol% isophthalate is accommodated without major disruption of the smectic and crystalline characteristics of PHBB. Copolymerization reduces the amount of LC character as indicated by thermal analysis, but does not affect the LC layer spacing in the WAXD pattern, which suggests that the isophthalate groups are excluded from the smectic layers. The resulting interruption of the smectic layer stacking leads to a reduction in lamellar thickness from 20 nm for PHBB to 12 nm for PHBB-10I. This corresponds to a reduction in the number of stacked layers from 11 to 6.

Both PHBB and PHBB-10I retain the lamellar and domain textures of the LC precursor upon crystallization [30–33]. Due to the extended chain conformation in the smectic state, crystallization may not require large axial shifts that would disrupt the smectic order, but rather only lateral translations and rotations about the chain axis. This is seen with the γ-crystal form of quenched PHBB and PHBB-10I, in which the chain is not fully extended. However, slow crystallization into the fully extended α-form requires larger rearrangements within the smectic lamellae. This disturbs the smectic order, as indicated by the weak or absent layer reflection in the WAXD pattern. However, even though the regular smectic stacking may be disrupted, AFM images reveal that the larger scale lamellar and domain textures of the LC precursor are preserved.

As the isophthalate content increases, more material is rejected from the smectic layers. First the interlamellar registry that gives rise to domains is lost, leaving a random array of short lamellae [5,9]. Quenched PHBB-30I and PHBB-50I fit this description, which suggests that these polymers crystallize from a melt with some LC character. Indeed, the smectic organization may facilitate crystallization. The double tan δ peak and intermediate free volume hole size of PHBB-30I suggest that some LC character persists in the non-crystalline regions. In contrast, the single strong tan δ peak and large hole size of PHBB-50I indicate that the non-crystalline regions of this copolymer are amorphous and do not retain any LC character.

With 75% isophthalate, runs of hexamethylene 4,4′-bibenzoate are not long enough or numerous enough to assemble as smectic layers, and PHBB-75I does not exhibit any LC character in DSC scans even when slowly cooled. Nevertheless, even PHBB-75I crystallizes from the glass in the PHBB α-form. Only quenched PHI takes a different crystal form. Both PHBB-75I and PHI crystallize in a manner that is typical of non-LC polymers as lamellar spherulites.

The persistence of LC character in copolymers with large amounts of the kinked isophthalate comonomer demonstrates the strong ordering tendency of bibenzoate, particularly with the 6-carbon hexamethylene spacer. Similarly, a large amount of 2,6-naphthalate, more than 60 mol%, was required to completely disrupt the smectic order of poly(hexamethylene 4,4′-bibenzoate-*co*-2,6-naphthalate) [34]. In contrast, only 30 mol% isophthalate destroyed the smectic character of poly(diethylene glycol 4,4′-bibenzoate-*co*-isophthalate) with a 5-atom spacer [5].

3.5. Oxygen transport properties

Typical experimental curves in Fig. 7 describe the oxygen flux $J(t)$ through PHBB, PHBB-I copolymers, and PHI at 23 °C. To facilitate comparisons among specimens that varied somewhat in thickness, the flux for a film of thickness 200 μm was calculated from Eq. (1) using values of P and D obtained from the measured flux and the original film thickness. The initial increase in oxygen flux reflected non-steady-state diffusion. This part of the curve was controlled mainly by the diffusivity D. As the permeant concentration in the specimen reached a constant distribution, the flux reached the steady-state value J_0. This value, normalized to the film thickness l and

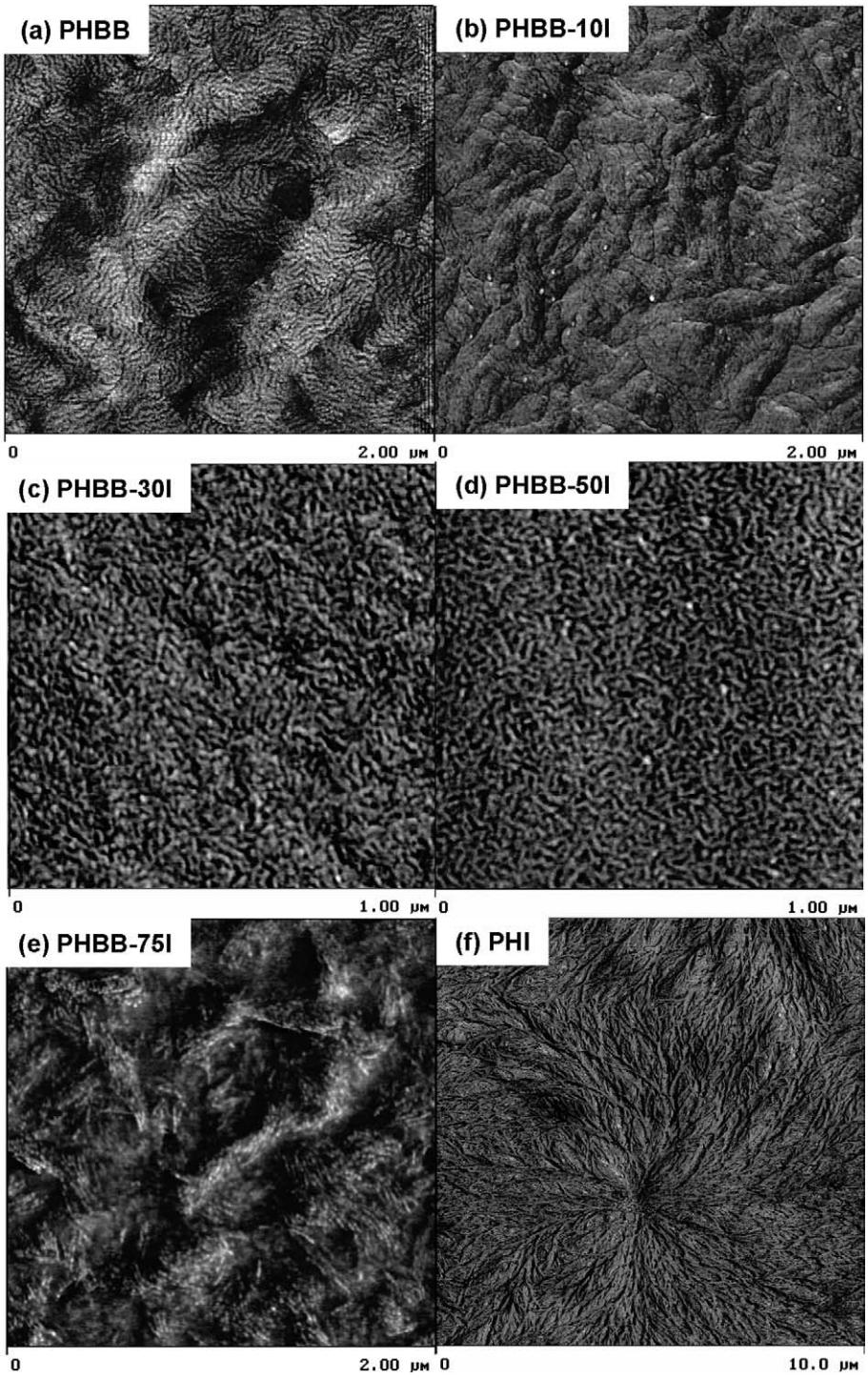

Fig. 6. AFM phase images of etched films. PHBB-75I and PHI were aged for 3 weeks after quenching.

the permeant gas pressure p, defined the permeability $P = J_0 l p^{-1}$. Comparison of flux curves indicated that incorporation of isophthalate up to 75 mol% sharpened the non-steady-state region (faster diffusion) and increased the steady-state flux (higher permeability). The lower steady-state flux of PHI compared to PHBB-75I reflected the higher crystallinity of PHI. The fit to the solution of Fick's second law (Eq. (1)) is included with the experimental points in Fig. 7. The two fitting parameters, P/l and D/l^2, were used to obtain diffusivity D and to accurately determine the permeability P. Solubility S was calculated from the relationship $S = PD^{-1}$.

The oxygen barrier properties at 23 °C are plotted in Fig. 8. The results are compiled in Table 1. Oxygen permeability of PHBB was 0.0906 cm^3 (STP) cm m^{-2} day^{-1} atm^{-1}, more than four times lower than that of glassy poly(ethylene terephthalate) (PET), 0.450 cm^3 (STP) cm m^{-2} day^{-1} atm^{-1} [5]. This was due

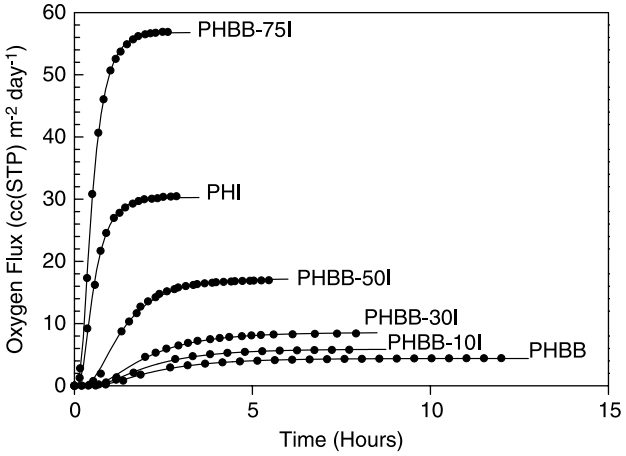

Fig. 7. Experimental $J(t)$ data obtained at 23 °C and the fit to Eq. (1).

to lower solubility, which is consistent with literature reports that very low gas solubility largely accounts for the exceptionally low gas permeability of LCPs compared to non-LC polymers [1–5]. Incorporation of isophthalate reduced LC order, and P increased steadily from 0.0906 for PHBB to 0.351 cm^3 (STP) cm m^{-2} day^{-1} atm^{-1} for PHBB-50I. Higher permeability was due to increases in both D and S. The large increase in D of PHBB-75I was due to the glass-to-rubber transition.

3.6. Oxygen sorption

The effect of the glass transition on oxygen solubility is shown in Fig. 9 by plotting S as a function the test temperature relative to the glass transition temperature (T_g–T_{test}). Data from the literature for numerous amorphous aromatic polyesters are included so that the plot covers a large range in (T_g–T_{test}) and encompasses T_g [35]. In the glassy state, as reflected by the right branch of the plot, oxygen sorption at low pressure is the

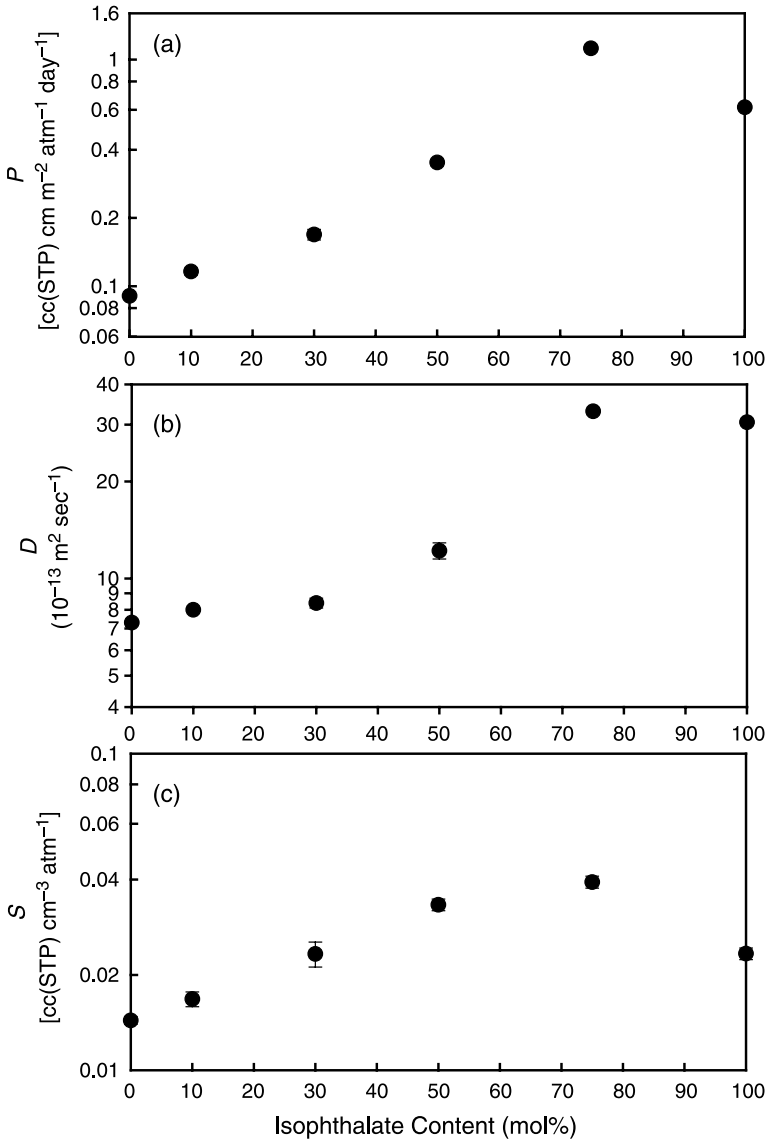

Fig. 8. Effect of isophthalate content on oxygen transport parameters at 23 °C (a) permeability; (b) diffusivity; and (c) solubility.

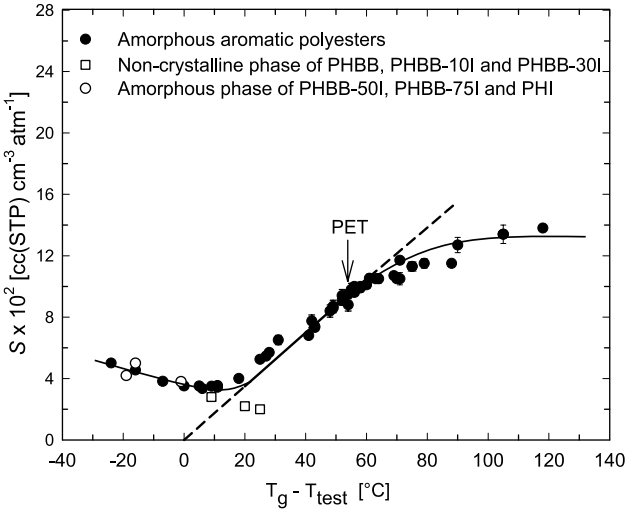

Fig. 9. Relationship between S and the difference (T_g–T_{test}). Solid symbols are taken from Ref. [35].

process of filling holes of excess free volume [36,44]. The amount of excess-hole free volume decreases as the temperature approaches T_g. This appears in Fig. 9 as a linear relationship between S and (T_g–T_{test}) that extrapolates to zero solubility at $T_{test}=T_g$ where the excess free volume is expected to disappear [37]. The slope gives the density of sorbed oxygen in the free volume holes [44]. Further from T_g, the decreasing slope indicates that the free volume approaches a constant value above the second-order transition at T_g-60 °C [44]. As T_{test} approaches T_g, the contribution of Henry's law sorption is responsible for deviation from the linear relationship. The oxygen solubility gradually increases as the temperature passes through T_g, which is reflected by the left branch in Fig. 9.

It is possible to extract the oxygen solubility in the non-crystalline regions from the measured values by considering the effect of crystallinity. Results for other bibenzoate polyesters support the simple two phase solubility model that considers an impermeable crystalline phase dispersed in a permeable amorphous or LC matrix [9,10]

$$S = S_m(1-\phi_c) \tag{2}$$

where S_m is the oxygen solubility of the non-crystalline LC or amorphous phase and ϕ_c is the volume fraction of crystallinity. Taking the crystallinity as estimated from WAXD, S_m was calculated from Eq. (2) and the results are included in Fig. 9 using T_g measured from DSC.

The solubility of oxygen in the non-crystalline regions of PHBB-50I, PHBB-75I and PHI conformed to the relationship between S and (T_g–T_{test}) established for amorphous glassy and rubbery polyesters, Fig. 9. This was consistent with the interpretation that the non-crystalline phase did not possess LC character even though PHBB-50I might have crystallized from the partially LC melt. On the other hand, S_m for PHBB and PHBB-10I was lower than expected based on amorphous polyesters. The low solubility of the non-crystalline LC phase was ascribed to smaller free volume hole size and possibly lower free volume hole density compared to an amorphous glass [5]. Again, PHBB-30I was intermediate between amorphous and LC behavior with solubility slightly lower than the established line.

3.7. Oxygen diffusivity

Oxygen diffusion in a glassy polymer is viewed as jumping from one free volume hole to another. The somewhat lower diffusivity of LC glasses compared to non-LC glasses reflects the combined effects of longer jump length and lower jump frequency [6]. A discussion of diffusivity measured at 23 °C is complicated by the glass-to-rubber transition, which occurs between PHBB-50I and PHBB-75I. A major change in the mechanism of gas transport occurs at T_g and concepts of diffusivity developed for the glassy state do not necessarily apply in the rubbery state. In addition, impermeable crystals impose a geometric impedance to the transport path that decreases D of PHBB, PHI and some of the copolymers. Because of the number of factors that affect D, only a qualitative structural interpretation is attempted.

The simple two-phase description of oxygen solubility is taken as the basis for examining the effect of crystallinity on D. The structural image of a crystallized LCP is one of small crystallites embedded in liquid crystalline lamellae [9]. Because of their low aspect ratio, the crystallites have a relatively small effect of D, especially when compared with the effect of the more conventional spherulitic morphology of non-LC crystalline polymers. Thus, crystallinity should have a relatively small effect on D of PHBB, but should have a larger effect on D of crystallized PHI.

Neglecting the effect of crystallinity, the amount of free volume is often related to D according to [38,39]

$$D \propto \exp\left[-\left(\frac{B}{\mathrm{FFV}}\right)\right] \tag{3}$$

where FVV is the fractional free volume and the constant B characterizes the size of the opening between polymer chains required for the penetrant molecule to pass. Although first developed for rubbery polymers, Eq. (3) was subsequently applied to glassy polymers as well [40,41]. Considerable scatter is encountered if Eq. (3) is tested against a large database encompassing various polymers and diffusants [42]. However, by limiting the analysis to a single system, a good correlation can be obtained [43]. It is noteworthy that an increase in free volume hole size parallels the trend in increasing D that accompanies the gradual loss of LC character (compare Fig. 5 with Fig. 8(b)). Lower FFV of the LC glass compared to the non-LC glass arises from smaller free volume hole size and lower free volume hole density [6].

In a glassy polymer, D also depends on the frequency with which the gas molecule jumps from one free volume hole to the next. Jump frequency depends on conformational changes and segmental motions of the polymer chain. In a glassy polyester, these thermal rearrangements manifest themselves as sub-T_g relaxation processes. A correlation between diffusivity and the

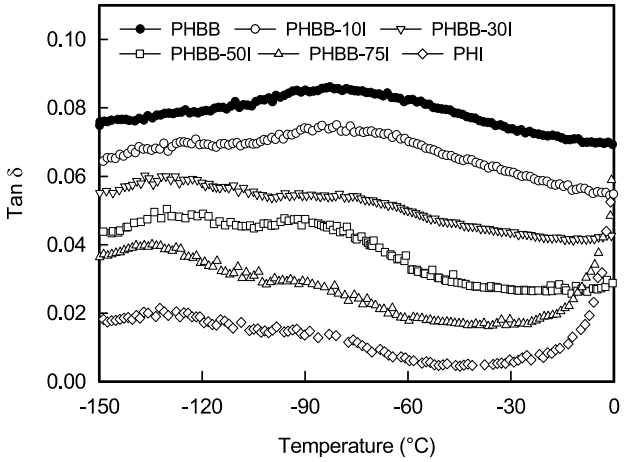

Fig. 10. DMTA tan δ curves showing the sub-ambient γ-relaxation region. The curves are shifted vertically.

γ-relaxation, particularly the relaxation component associated with gauche conformations of the glycol, exists for various aromatic polyesters [10,44–46].

The sub-ambient γ-relaxation in the -70 to -120 °C range is characteristic of aromatic polyesters with flexible spacers, Fig. 10. The complexity of the γ-relaxation leads to identification of a higher temperature component (γ_1 at about -80 °C) with trans conformations of the spacer and a lower temperature component (γ_2 at about -130 °C) with gauche conformations of the spacer [47] The tan δ curve of PHBB shows primarily the γ_1 component, which is consistent with the extended conformation of the LC chains, Fig. 10. With increasing isophthalate content, the γ_2 component increases in intensity relative to the γ_1 component until it becomes the strongest component in the relaxation spectra of PHBB-30I and PHBB-50I. This is consistent with an increase in gauche conformations as the non-crystalline chains lose the extended LC conformation. The increase in γ_2 intensity parallels the increase in D. The same qualitative relationship between D and γ_2 intensity has been reported for other polyesters based on bibenzoate [10].

4. Conclusions

It is axiomatic that copolymerization disrupts long range LC order. However, in some cases a surprisingly large faction of a non-LC comonomer can be incorporated before the LC order is completely destroyed. This appears to be particularly the case with copolyesters based on 4,4′-bibenzoate. In the present study, copolymers with the hexamethylene spacer and up to 50 mol% isophthalate give evidence of LC character in the precursor melt. Further evidence for the accommodating nature of ordered bibenzoate structures is provided by crystallization of a copolymer with 75 mol% isophthalate in the PHBB α-crystal form with only small perturbations of the unit cell.

Polymers with LC character are known to have low gas permeability. Copolymers in which the amount of LC character can be systematically changed are particularly attractive for examining the role of LC character in achieving low gas permeability. It is confirmed here that both S and D for oxygen are affected. Mechanistically, oxygen sorption in the glass is viewed as the filling of excess free volume holes. Smaller free volume hole size of the smectic glass compared to the amorphous glass, and possibly lower free volume hole density, give rise to lower oxygen solubility. Diffusivity derives from jumps of the gas molecule between free volume holes, and depends on the amount of free volume and on the segmental motions that manifest themselves as sub-T_g relaxations, particularly the relaxation component associated with gauche conformations of the glycol. Results from this study provide further evidence that the extended LC chain conformation reduces the fraction of glycol units in gauche conformations and thereby reduces oxygen diffusivity.

Acknowledgements

The authors thank Professor D.A. Schiraldi for assistance in obtaining the polymers. Modern Controls, Inc., is thanked for generous support of the facility for gas transport studies at Case Western Reserve University.

References

[1] Chiou JS, Paul DR. J Polym Sci, Part B: Polym Phys 1987;25:1699–707.
[2] Weinkauf DH, Paul DR. J Polym Sci, Part B: Polym Phys 1991;29:329–40.
[3] Weinkauf DH, Paul DR. J Polym Sci, Part B: Polym Phys 1992;30:817–35.
[4] Weinkauf DH, Paul DR. J Polym Sci, Part B: Polym Phys 1992;30:837–49.
[5] Hu YS, Liu RYF, Schiraldi DA, Hiltner A, Baer E. Macromolecules 2004;37:2128–35.
[6] Hu YS, Liu RYF, Schiraldi DA, Hiltner A, Baer E. Macromolecules 2004;37:2136–43.
[7] Jackson Jr WJ, Morris JC. In: Weiss RA, Ober CK, editors. Liquid–crystalline polymers. Washington, DC: American Chemical Society; 1990. p. 16–32 [chapter 2].
[8] Ma H, Hibbs M, Collard DM, Kumar S, Schiraldi DA. Macromolecules 2002;35:5123–30.
[9] Hu YS, Schiraldi DA, Hiltner A, Baer E. Macromolecules 2004;36:3606–15.
[10] Hu YS, Hiltner A, Baer E. Polymer; in press.
[11] Krigbaum WR, Asrar J, Toriumi H, Ciferri A, Preston J. J Polym Sci, Polym Lett Ed 1982;20:109–15.
[12] Meurisse P, Noel C, Monnerie L, Fayolle B. Br Polym J 1981;13:55–63.
[13] Watanabe J, Hayashi M, Nakata T, Niori T, Tokita M. Prog Polym Sci 1997;22:1053–87.
[14] Krigbaum WR, Watanabe J. Polymer 1983;24:1299–307.
[15] Li X, Brisse F. Macromolecules 1994;27:7725–34.
[16] Higuchi H, Yu Z, Jamieson AM, Simha R, McGervey JD. J Polym Sci, Part B: Polym Phys 1995;33:2295–305.
[17] Sekelik DJ, Stepanov SV, Nazarenko S, Schiraldi D, Hiltner A, Baer E. J Polym Sci, Part B: Polym Phys 1999;37:847–57.
[18] Watanabe J, Hayashi M. Macromolecules 1988;21:4083–8.
[19] Abe A. Macromolecules 1984;17:2280–7.
[20] Watanabe J, Hayashi M. Macromolecules 1988;21:278–80.
[21] Benavente R, Pereña JM, Pérez E, Bello A. Polymer 1993;34:2344–7.
[22] Benavente R, Pereña JM, Pérez E, Bello A. Polymer 1994;35:3686–90.
[23] Tsukruk VV, Shilov VV, Lipatov YS. Acta Polym 1985;36:403–12.
[24] Mazelet G, Kléman M. J Mater Sci 1988;23:3055–60.

[25] Ford JR, Bassett DC, Mitchell GR. Mol Cryst Liq Cryst 1990;180B: 233–43.
[26] Wang W, Lieser G, Wegner G. Macromolecules 1994;27:1027–32.
[27] Takahashi T, Nagata F. J Macromol Sci, Phys 1989;B28:349–64.
[28] Tokita M, Takahashi T, Hayashi M, Inomata K, Watanabe J. Macromolecules 1996;91:1345–8.
[29] Tokita M, Osada K, Watanabe J. Liq Cryst 1997;23:453–6.
[30] Warner SB, Jaffe M. J Cryst Growth 1980;48:184–90.
[31] Cheng SZD, Yandrasits MA, Percec V. Polymer 1991;32:1284–92.
[32] Pardey R, Zhang A, Gabori PA, Harris FW, Cheng SZD, Adduci J, et al. Macromolecules 1992;25:5060–8.
[33] Heberer D, Keller A, Percec V. J Polym Sci, Part B: Polym Phys 1995;33: 1877–94.
[34] Tokita M, Osada K, Watanabe J. Polym J 1998;30:589–95.
[35] Hiltner A, Liu RYF, Hu YS, Baer E. J Polym Sci, Part B: Polym Phys 2005;43:1047–63.
[36] Weiss GH, Bendler JT, Shlesinger MF. Macromolecules 1992;25:990–2.
[37] Vrentas JS, Duda JL. J Appl Polym Sci 1978;22:2325–39.
[38] Cohen MH, Turnbull D. J Chem Phys 1959;31:1164–9.
[39] Takeuchi H, Okazaki K. J Chem Phys 1990;92:5643–52.
[40] Duda JL, Zielinski JM. In: Neogi P, editor. Diffusion in polymers. New York: Marcel Dekker; 1996. p. 143–71 [chapter 3].
[41] Park JY, Paul DR. J Membr Sci 1997;125:23–39.
[42] Thran A, Kroll G, Faupel F. J Polym Sci, Part B: Polym Phys 1999;37: 3344–58.
[43] Hu YS, Liu RYF, Zhang LQ, Rogunova M, Schiraldi DA, Nazarenko S, et al. Macromolecules 2002;35:7326–37.
[44] Polyakova A, Liu RYF, Schiraldi DA, Hiltner A, Baer E. J Polym Sci, Part B: Polym Phys 2001;39:1889–99.
[45] Polyakova A, Connor DM, Collard DM, Schiraldi DA, Hiltner A, Baer E. J Polym Sci, Part B: Polym Phys 2001;39:1900–10.
[46] Andrade GS, Collard DM, Schiraldi DA, Hu YS, Baer E, Hiltner A. J Appl Polym Sci 2003;89:934–42.
[47] Hiltner A, Baer E. J Macromol Sci, Phys 1972;B6:545–58.